

Model-independent constraints on modified gravity from current data and from the Euclid and SKA future surveys.

Laura Taddei, Matteo Martinelli, Luca Amendola

Institut für Theoretische Physik, Ruprecht-Karls-Universität Heidelberg, Philosophenweg 16, 69120 Heidelberg, Germany.

E-mail: taddei@thphys.uni-heidelberg.de, martinelli@lorentz.leidenuniv.nl, amendola@thphys.uni-heidelberg.de

Abstract. The aim of this paper is to constrain modified gravity with redshift space distortion observations and supernovae measurements. Compared with a standard Λ CDM analysis, we include three additional free parameters, namely the initial conditions of the matter perturbations, the overall perturbation normalization, and a scale-dependent modified gravity parameter modifying the Poisson equation, in an attempt to perform a more model-independent analysis. First, we constrain the Poisson parameter Y (also called G_{eff}) by using currently available $f\sigma_8$ data and the recent SN catalog JLA. We find that the inclusion of the additional free parameters makes the constraints significantly weaker than when fixing them to the standard cosmological value. Second, we forecast future constraints on Y by using the predicted growth-rate data for Euclid and SKA missions. Here again we point out the weakening of the constraints when the additional parameters are included. Finally, we adopt as modified gravity Poisson parameter the specific Horndeski form, and use scale-dependent forecasts to build an exclusion plot for the Yukawa potential akin to the ones realized in laboratory experiments, both for the Euclid and the SKA surveys.

Contents

1	Introduction	1
2	Linear perturbations	3
3	Likelihood analysis	5
4	Current data	6
5	Forecast data	8
6	A cosmological exclusion plot	14
7	Conclusions	18
8	Acknowledgments	19

1 Introduction

Since its discovery in 1998 [1, 2], the accelerated expansion of the Universe has remained an open problem of cosmology, as our General Relativity based description of the Universe only allows for deceleration unless some additional components, such as a cosmological constant Λ or additional fundamental fields, are added to the theory. The additional fields might also modify the effective gravitational potential and give rise to so-called “modified gravity” (MG) models. This has prompted cosmologists to investigate many alternatives to General Relativity (see e.g. [3] for an overview of currently available models). Current and upcoming cosmological surveys are finally reaching a sensitivity which will allow to test modifications of gravity at cosmological scales and possibly to distinguish these from the simple scenario of a constant energy density (Λ CDM model) or uncoupled and unclustered dark energy.

In general, at linear perturbation level, a modification of scalar perturbations with respect to the Λ CDM model can be described by two functions in the Einstein equations, which generally depend on time and space or, in Fourier space, on the wavenumber k (see for instance [4]). One function is $Y(t, k)$ which modifies the standard Poisson equation (and also Newton’s constant, so it is often denoted as G_{eff} : this notation however can be confusing since if Y is scale dependent, the expression for G_{eff} in the potential and in the force equations are different). The other one is the anisotropic stress $\eta(t, k)$, which is the ratio between the two linear gravitational potentials Φ and Ψ which enter the spatial and temporal part, respectively, of the perturbed Friedmann-Robertson-Walker (FRW) metric. (Note that our perturbation variables are to be thought of as the root mean square of the corresponding random variable, so they are positive defined.) In standard gravity, we have $Y = \eta = 1$.

For a non-relativistic perfect fluid, the anisotropic stress is not sourced by matter at the linear level, so in this case η is a genuine indicator of modified gravity [5]. In [6], the authors employed a model-independent approach to measure η without any assumption on the initial spectrum of perturbations and the bias, finding a forecasted error of a few percent if η is assumed constant. On the other hand, $Y \neq 1$ can in principle arise also due to clustering of dark energy, rather than to a modification of gravity, but if the dark energy field is not

coupled to matter the clustering on sub-horizon scales is expected to be negligible unless the field mass is so large that the field behaves as dark matter and therefore does not drive acceleration, or the sound speed is extremely small (orders of magnitudes smaller than the velocity of light). In any case, the detection of a deviation of Y from unity would signal an important manifestation of new physics.

In a large class of scalar field models, the so-called Horndeski Lagrangian, the two functions Y, η take a particular simple form in the quasi-static limit, i.e. when we neglect the time-derivatives of the perturbation variables (see next section). This is a good approximation for scales much below the sound horizon, see e.g. [7–9]. For our purposes we assume this approximation to hold; however, it is worth stressing that this point should be further addressed, specially given the large scales probed by the survey we will discuss in the rest of the paper (see e.g. [10]). In real space, the Horndeski form gives rise to the Yukawa correction to the Newtonian potential. This paper is devoted to constraining the quasi-static scale-dependent form for the Yukawa parameters through current and future redshift space distortion (RSD) and supernovae data.

The parameter Y enters the equation for the growth of matter perturbation density contrast δ_m . By comparing the theoretical prediction of the growth of δ_m with the observations provided by the redshift distortion quantity $f\sigma_8(z)$ one can constrain the modified gravity parameters. However, one needs also to assume an initial condition for δ in order to integrate the differential equation. Almost universally, the choice has been to assume a standard matter-dominated cosmology at high redshift. This choice, however, is a very special one and is not justified neither by observations nor by theory. On the observational side, there is no direct information on the growth of matter at any epoch between the cosmic microwave background (CMB) at $z \approx 1000$ and $z \approx 1$, but only integral information like the integrated Sachs-Wolfe effect or the CMB lensing. On the theory side, any model in which dark energy is not negligible during the matter era will introduce a deviation from standard initial conditions that should be taken into account (see discussion in [11]).

A further problem arises when using the $f\sigma_8(z)$ data. In fact, the quantity that is observed is the redshift-distorted galaxy power spectrum, namely

$$P_g(z, k, \mu) = \left(1 + \frac{f(z, k)}{b(z, k)}\mu^2\right)^2 G^2(z, k) \sigma_8^2 b^2(z, k) P_m(k) \quad (1.1)$$

where $f = d \log \delta_m / d \log a$ is the growth rate, $b(z, k)$ is the bias function, $G(z, k) = \delta_m(z, k) / \delta_m(0, k)$ is the growth function, μ is the direction cosine between the line of sight and the wave vector \vec{k} , and $P_m = \delta_m(0, k)^2$ is the present matter power spectrum. Taking $P_g^{1/2}(z, k, 1) - P_g^{1/2}(z, k, 0)$ one gets

$$f(z, k)G(z, k)\sigma_8 P_m^{1/2}(k) = f\sigma_8(z) \times P_m^{1/2}(k) = \sigma_8 \delta'_m \quad (1.2)$$

(the prime denotes derivative with respect to $\log a$ and $\sigma_8(z) \equiv \sigma_8 G$). This is the raw observed quantity. In order to obtain $f\sigma_8(z)$ one needs a model for $P_m^{1/2}(k)$ and at this point the assumption of a standard power spectrum shape is inserted in the procedure. The initial power spectrum shape can be measured or constrained through CMB observations but nothing guarantees that the shape has not changed after recombination, unless we assume again a standard matter era. The two problems just mentioned can be both seen as initial conditions problems: the equation for δ_m is second order (see next section) so we need two free initial conditions, δ_{in} and δ'_{in} , in order to carry out a more model-independent estimation of modified gravity parameters. Of course one is perfectly entitled to stick with a standard

matter era throughout, but one should be aware that in this case one is testing a combination of standard assumptions and new physics, and the constraints on the MG parameters will change when assuming a different matter era. The purpose of this paper is to investigate possible constraints from future surveys, when these common assumptions are removed, thus performing a rather model independent forecast on general MG theories.

While at first we explore the simplest case in which Y is constant both in space and time, we then move to the Horndeski scale-dependent form, still freezing the time behavior. In this way we can constrain the parameters that enter the Yukawa potential and build a forecast exclusion plot similar to the one realized in laboratory or within the solar system. We follow here the same approach employed in [11], extending the analysis performed there to more general expansion histories, in order to take into account models which deviate from Λ CDM also at the background level. For this purpose we use a CPL form [12] for the Dark Energy equation of state parameter $w(z)$ and we include supernovae data in order to better constrain the background. Furthermore we also analyze SKA-like data alongside a Euclid-like survey.

It is important to remark that in the forecasts for Euclid and SKA we combine galaxy clustering and lensing (shear) in a non-parametric way to predict the measurement errors on the RSD quantity $f\sigma_8(z)$ and on the expansion rate $E(z) \equiv H(z)/H_0$, as shown in [6]. Lensing measures the lensing potential and the expansion rate, while galaxy clustering measures the amplitude of the Newtonian potential, the RSD $f\sigma_8(z)$ and the expansion rate. The resulting Fisher matrix is marginalised over the lensing potential and over the spectrum amplitude to obtain the forecasted error on $f\sigma_8(z), E(z)$. These two quantities are model-independent in the sense that they do not depend on the power spectrum shape ($f\sigma_8(z)$ becomes model independent after marginalising over an overall constant, as explained later on), nor on the model of galaxy bias. We then use exclusively these two quantities to obtain constraints on the cosmological and modified gravity parameters. This ensures that our final constraints are model-independent in the sense explained above. The price to pay is that the constraints might become weaker than shown in other papers that assume either specific spectra shapes (e.g. Λ CDM), or bias models, or restrict in some way the modified gravity sector.

2 Linear perturbations

We focus our attention on the evolution of linear perturbations in the quasi-static limit (i.e. for scales significantly inside the sound horizon, $c_s k/(aH) \gg 1$), such that the terms containing k dominate over the time-derivative terms.

As shown in [8], for a general modified gravity theory, one has the following equation for linear perturbation growth:

$$\delta_m'' + \left(2 + \frac{E'}{E}\right)\delta_m' = \frac{3}{2}\Omega_m\delta_m Y(a, k), \quad (2.1)$$

where δ_m is the matter density contrast, $\Omega_m = \Omega_{m0}a^{-3}/E^2$ is the matter density parameter and $E \equiv H/H_0$ is the dimensionless Hubble function, which describes the background expansion. The function Y represents the effective gravitational constant for matter and it is defined as

$$Y(a, k) = -\frac{2k^2\Psi}{3(aH)^2\Omega_m\delta_m} \quad (2.2)$$

As done previously [11], we assume either that baryons do not feel modified gravity (i.e., there is a suitable conformal or disformal factor in the metric coupled to baryons that cancel the effects of modified gravity) or that the local gravity experiments occur in an environments where the extra force is negligible (screening mechanism). In either case, we can escape most local gravity constraints. The time variation of the product GM is not screened, so one still has to confront with local constraints at the present time. However, one might always design a "time-screened" model such that the present constraints on $(\dot{GM})/(GM)$ vanish while being significant in the past, so again local constraints can always be avoided. We will therefore neglect any local constraint in this paper.

The background expansion is described by:

$$E^2 = \Omega_{m,0}(1+z)^3 + (1 - \Omega_{m,0})e^{3\int(1+w(z'))/(1+z')dz'} \quad (2.3)$$

in which we consider the Chevallier-Polarski-Linder parametrization [12] for the dark energy equation of state:

$$w(z) = w_0 + w_a \frac{z}{(1+z)}. \quad (2.4)$$

Therefore Eq. (2.1) can be written as

$$\delta_m'' + \left(2 + \frac{E'}{E}\right)\delta_m' = \frac{3}{2} \frac{\delta_m}{a^3 E^2} \Omega_{m,0} Y. \quad (2.5)$$

As in [11], we define the initial conditions parameter $\alpha \equiv \delta_{in}'/\delta_{in}$. When we solve Eq. (2.5), we choose the initial value at $z_{in} \approx 3.5$, just beyond the observed range. We assume for now Y to be constant in space and time. The equation is then k -independent and the result can be directly compared to observations that are obtained in a finite range of scales. The constant α can itself in principle be scale dependent but for simplicity we assume this to not be the case. Since observations have so far been performed in a relatively small range of scales, this simplification is probably not very harmful at least for as concerns current constraints.

In total we have five parameters $\{\Omega_{m,0}, w_0, w_a, Y, \alpha\}$, where only the first three enter the background equation (Eq. (2.3)), plus an overall constant for growth data that we can marginalize over analytically. We adopt uniform flat prior probabilities allowing for fairly large ranges (several σ larger than current constraints) as we expect degeneracies between standard and modified gravity parameters to widen the region of the parameter space with a non vanishing likelihood. The parameter space is sampled both through a grid approach and with an MCMC approach through the publicly available package `cosmomc` [13], with a convergence diagnostic using the Gelman and Rubin statistic. We have thoroughly checked that the two approaches give compatible results and we will use those obtained with the latter throughout this paper.

Later on, we will take the Horndeski space-dependent form and we will have to define the k -ranges. In this case the expression for Y in the quasi-static limit can be written as [8]

$$Y = h_1 \frac{1 + (k/k_p)^2 h_5}{1 + (k/k_p)^2 h_3} \quad (2.6)$$

where h_1, h_3, h_5 are time dependent functions that can be explicitly obtained when the full Horndeski Lagrangian is given [5]. The scale k_p is an arbitrary pivot scale that we choose to be $k_p = 1h/\text{Mpc}$.

3 Likelihood analysis

We describe the growth rate data as a set of values $f\sigma_{8i}$ at various redshifts, defined as:

$$f\sigma_{8i} = f(z_i)\sigma_8(z_i) = f(z_i)\sigma_8 G(z_i) = \sigma_8 \frac{\delta'_i}{\delta_0} = \sigma_8 d_i \quad (3.1)$$

where $d_i = \delta'_i/\delta_0$. The growth-rate theoretical estimates are defined as $\hat{d}_i = \hat{\delta}'_i/\hat{\delta}_0$, where $\hat{\delta}$ is the solution of Eq. (2.5). Also for the background, we can define the data E_i and the theoretical estimates \hat{E}_i , given by Eq. (2.3), calculated for every redshift values. We build then the $\bar{\chi}^2$ function:

$$\bar{\chi}^2 = (\vec{d}_i - \vec{t}_i) C_{ij}^{-1} (\vec{d}_j - \vec{t}_j) \quad (3.2)$$

in which the data vector \vec{d}_i contains $\{f\sigma_{8i}; E_i\}$, \vec{t}_i includes $\{\hat{d}_i; \hat{E}_i\}$ for each value of redshift z_i and C_{ij} is the covariance matrix of the data. We decompose C_{ij}^{-1} into three sub-matrices (RR) , (ER) , (EE) as

$$C_{ij}^{-1} = \begin{pmatrix} (RR)_{ij} & (ER)_{ij} \\ (ER)_{ij} & (EE)_{ij} \end{pmatrix} \quad (3.3)$$

They are respectively the growth-rate error matrix $(RR)_{ij}$, the background error matrix $(EE)_{ij}$ and the mixing matrix between the growth-rate and the background errors $(ER)_{ij}$.

As mentioned in the Introduction, the data $f\sigma_8(z)$ are defined up to a constant that depends on the choice of the shape of the power spectrum. Here we wish to remain as much model-independent as possible and therefore we marginalize over this overall constant. Once again, in principle the constant might be scale dependent but we simplify our task by assuming it is not. Our goal, after all, is to see how much the constraints change when some of the model-dependent assumptions are removed and it is sufficient for now to show the effect when just a minimal set of assumptions are removed.

We marginalize then the likelihood $L' = \exp(-\bar{\chi}^2/2)$ over an overall positive factor with a uniform prior; this leads to a new posterior $L = \exp(-\chi^2/2)$ where

$$\chi^2 = S_{tt} - \frac{S_{dt}^2}{S_{dd}} - 2 \log \left(1 + \text{Erf} \left(\frac{S_{dt}}{\sqrt{2S_{dd}}} \right) \right) \quad (3.4)$$

and:

$$S_{dt} = d_i (RR)_{ij} \hat{d}_j + (\hat{E}_i - E_i) (ER)_{ij} d_j \quad (3.5)$$

$$S_{dd} = d_i (RR)_{ij} d_j \quad (3.6)$$

$$S_{tt} = (E_i - \hat{E}_i) (EE)_{ij} (E_j - \hat{E}_j) - 2(E_i - \hat{E}_i) (ER)_{ij} \hat{d}_j + \hat{d}_i (RR)_{ij} \hat{d}_j \quad (3.7)$$

This is the likelihood we will employ when forecasting constraints from future experiments.

When estimating the forecast constrains from clustering and lensing, we assume $E(z)$ as a free parameter in each bin, and therefore the final constraints on $E(z)$ will be correlated with thos on the clustering and lensing variables. Current data, however, are produced in such a way that $E(z)$ either does not enter the analysis or is fixed to Λ CDM. In both cases, it is not correlated with the growth data. The procedure for the current data is therefore slightly different and will be discussed next.

4 Current data

Supernovae data

In order to constrain the background, we will use the most recent SN catalog dubbed JLA (acronym for Joint Lightcurve Analysis [14]). This is a joint analysis of the 740 spectroscopically confirmed supernovae type Ia of the SNLS and SDSS-II collaborations and covers a redshift range from 0.02 to 1.3. We can define the predicted magnitudes $m(z_i)_{th}$ by:

$$m(z_i)_{th} = M + 5 \log_{10} d_L(z_i) + 25 \quad (4.1)$$

where $d_L(z)$ is the luminosity distance, which is computed under the assumption of spatial flatness:

$$d_L(z) = \frac{(1+z)}{H_0} \int_0^z \frac{dz'}{E(z')} \quad (4.2)$$

and M is the absolute magnitude. We can rewrite Eq. (4.1) as $m(z_i)_{th} = \mu(z_i)_{th} + \gamma$, where $\mu(z_i)_{th} = 5 \log_{10} \hat{d}_L(z_i)$ (with $\hat{d}_L \equiv d_L H_0$) and $\gamma = M + 25 - 5 \log_{10} H_0$. We note that, instead of the background theoretical estimates of E_i , we have the theoretical estimates of the apparent magnitude, defined in Eq. (4.1).

The observed apparent magnitude m_i is given by [14]:

$$m = m_B^* - M_B + \alpha X_1 - \beta C \quad (4.3)$$

where m_B^* corresponds to the observed peak magnitude in the rest-frame B band, X_1 and C describe, respectively, the time stretching of the light-curve and the supernova color at maximum brightness, and α, β, M_B are nuisance parameters related to the distance estimate, which are added to the sampled parameters and then marginalized out. The analysis for the supernovae is based on the χ'^2 function:

$$\chi'^2_{SNIa} = \sum_i \frac{[m_i - \mu(z_i)_{th} - \gamma]^2}{\sigma_i^2} \quad (4.4)$$

where σ_i are the errors on the apparent magnitudes and the index i labels the elements of the JLA dataset. We marginalize the likelihood $L'_{SNIa} = \exp(-\chi'^2_{SNIa}/2)$ over γ [3], leading to a new marginalized χ^2 function:

$$\chi^2_{SNIa} = \left(S_2 - \frac{S_1^2}{S_0} \right) \quad (4.5)$$

where the quantities S_n are defined as:

$$S_n \equiv \sum_i \frac{[m_i - \mu(z_i)_{th}]^n}{\sigma_i^2}. \quad (4.6)$$

Growth data

The current dataset includes all the independent published estimates of $f\sigma_8(z)$ obtained with the redshift distortion method. It includes the data from 2dFGS, 6dFGS, LRG, BOSS, CMASS, WiggleZ and VIPERS, and spans the redshift interval from $z = 0.07$ to $z = 0.8$, see

Survey	z	$f(z) \sigma_8(z)$	References
6dFGRS	0.067	0.423 ± 0.055	Beutler et al. (2012) [17]
LRG-200	0.25	0.3512 ± 0.0583	Samushia et al (2012) [18]
	0.37	0.4602 ± 0.0378	
LRG-60	0.25*	0.3665 ± 0.0601	Samushia et al (2012) [18]
	0.37*	0.4031 ± 0.0586	
BOSS	1) 0.30	$0.408 \pm 0.0552, \rho_{12} = -0.19$	Tojeiro et al. (2012)[19]
	2) 0.60	0.433 ± 0.0662	
WiggleZ	1) 0.44	$0.413 \pm 0.080, \rho_{12} = 0.51$	Blake (2011) [20]
	2) 0.60	$0.390 \pm 0.063, \rho_{23} = 0.56$	
	3) 0.73	0.437 ± 0.072	
Vipers	0.8	0.47 ± 0.08	De la Torre et al (2013)[21]
2dFGRS	0.17	0.51 ± 0.06	Percival et al. (2004) [22][23]
LRG	0.35	0.429 ± 0.089	Chuang and Wang (2013) [24]
LOWZ	0.32	0.384 ± 0.095	Chuang et al (2013)[25]
CMASS	0.57*	0.348 ± 0.071	
	0.57*	0.423 ± 0.052	Beutler et al (2014)[26]
	0.57	0.441 ± 0.043	Samushia et al (2014) [27]
	0.57*	0.450 ± 0.011	Reid et al (2013)[28]

Table 1. Current published values of $f\sigma_8(z)$. In some cases we list also the correlation coefficient ρ_{ij} between different bins [15]. When there are different published results from the same dataset, we include only the more recent one (we put an asterisk to the entries which are not employed in this analysis).

Table 1 (see also [15, 16]). In some cases the correlation coefficient between two samples has been estimated in [15] and included in our analysis; when there are different published results from the same dataset in Table 1, we include only the more recent one.

The χ^2_{growth} can be expressed as in Eq.(3.4) with coefficients

$$S_{dt} = d_i(RR)_{ij} \hat{d}_j \quad (4.7)$$

$$S_{dd} = d_i(RR)_{ij} d_j \quad (4.8)$$

$$S_{tt} = \hat{d}_i(RR)_{ij} \hat{d}_j \quad (4.9)$$

We can then combine these data with the marginalized SN χ^2 of Eq.(4.4) to include information on the background

$$\chi^2 = \chi^2_{growth} + \chi^2_{SNIa} \quad (4.10)$$

Results

We now analyze current data using the prescription of Eq.(4.10) in two different cases: the Λ CDM case, in which we fix $Y = 1$ and $\alpha = 1$, and the case where the additional parameters are free to vary, from now on denoted “MG case”.

Table 2 and Fig. 1 show the results obtained for these two analysis; the top panels of Fig. 1 highlight how the inclusions of Y and α in the analysis bring to looser constraints on standard cosmological parameters due the degeneracies highlighted in the bottom panel. In

Current Data	$\Omega_{m,0}$	w_0	w_a	Y	α
Λ CDM case	< 0.273	$-0.71^{+0.16}_{-0.11}$	$0.17^{+0.71}_{-0.53}$	fixed to 1	fixed to 1
MG case	< 0.409	$-0.79^{+0.24}_{-0.11}$	$-0.29^{+1.4}_{-0.52}$	< 2.22	$0.21^{+0.21}_{-0.72}$

Table 2. Marginalized values and 1- σ errors on the free parameters for current data in the Λ CDM case and in the MG case. When a two-tail likelihood is not allowed by the data, the 2- σ upper limit is shown.

particular, with respect to the Λ CDM case, the 2- σ bound on Ω_m increases by 41%, while the 1- σ error on w_0 and w_a increases by 44% and 53% respectively. Furthermore, it is interesting to notice how the inclusion of MG parameters relaxes the slight tension of current data with the Λ CDM background ($w_0 = -1$, $w_a = 0$) at the cost of non standard best fit values for Y and α .

Fig. 2 shows the posterior distribution obtained on $\Omega_{m,0}$ through growth data, supernovae and their combination in the MG case; it is interesting to notice that the growth rate data tend to move the marginalized 1-dimensional posterior for $\Omega_{m,0}$ toward smaller values, while supernovae data support a maximum near $\Omega_{m,0} = 0.3$. The combined analysis still prefers low values of the matter density, but the effect of supernovae is to make more likely also higher values with respect to the growth-data-only analysis. This effect is stronger in the MG case as the degeneracies of Y and α with $\Omega_{m,0}$ degrade the constraining power of growth data on the matter density, increasing therefore the statistical significance of the SN dataset.

Fig. 3 shows the best fit $f\sigma_8(z)$ trends found with our analysis (both in the Λ CDM and MG cases) compared to the $f\sigma_8(z)$ predicted using the best fit results of Planck 2015 [29]. Our marginalization over σ_8 allows to rescale the theoretical $f\sigma_8(z)$ by an arbitrary factor and this allows non standard values of $\Omega_{m,0}$ and w_0 , w_a to better fit the data; comparing the obtained best fit χ^2 values with the one given by the Planck best fit parameters, we find $\Delta\chi^2 = -2.57$ in the Λ CDM case, while allowing also for Y and α to vary we obtain an improvement $\Delta\chi^2 = -3.25$.

5 Forecast data

Euclid mission

After having obtained constraints from currently available data, it is interesting to investigate how future surveys can improve our tests of gravity. To this purpose we focus on the future ESA mission Euclid, using the specifications presented in [30], i.e. a coverage of 15,000 square degrees and a redshift interval $z = 0.5 - 1.5$. In order to forecast $f\sigma_8$ data from this survey, we follow the z -binning procedure of [6] and we divide the redshift range in equally spaced bins of width $\Delta z = 0.2$ and, in order to prevent accidental degeneracy due to low statistic, a single larger redshift bin between $z = 1.5 - 2.1$, for a total of six bins. As we are mainly interested in the effect of the theory approach generality on constraints, we limit our analysis to the nominal Euclid specifications [30]; however, recently the modelling of $H\alpha$ emitters luminosity function has been discussed [31] and we emphasize that also this more conservative approach in forecasting the amount of observed sources might have a significant effect on the expect results.

Beside this, we also include in our forecast the Euclid weak lensing forecasts, following the prescription of [6], where the full Fisher matrix for redshift distortion, galaxy clustering

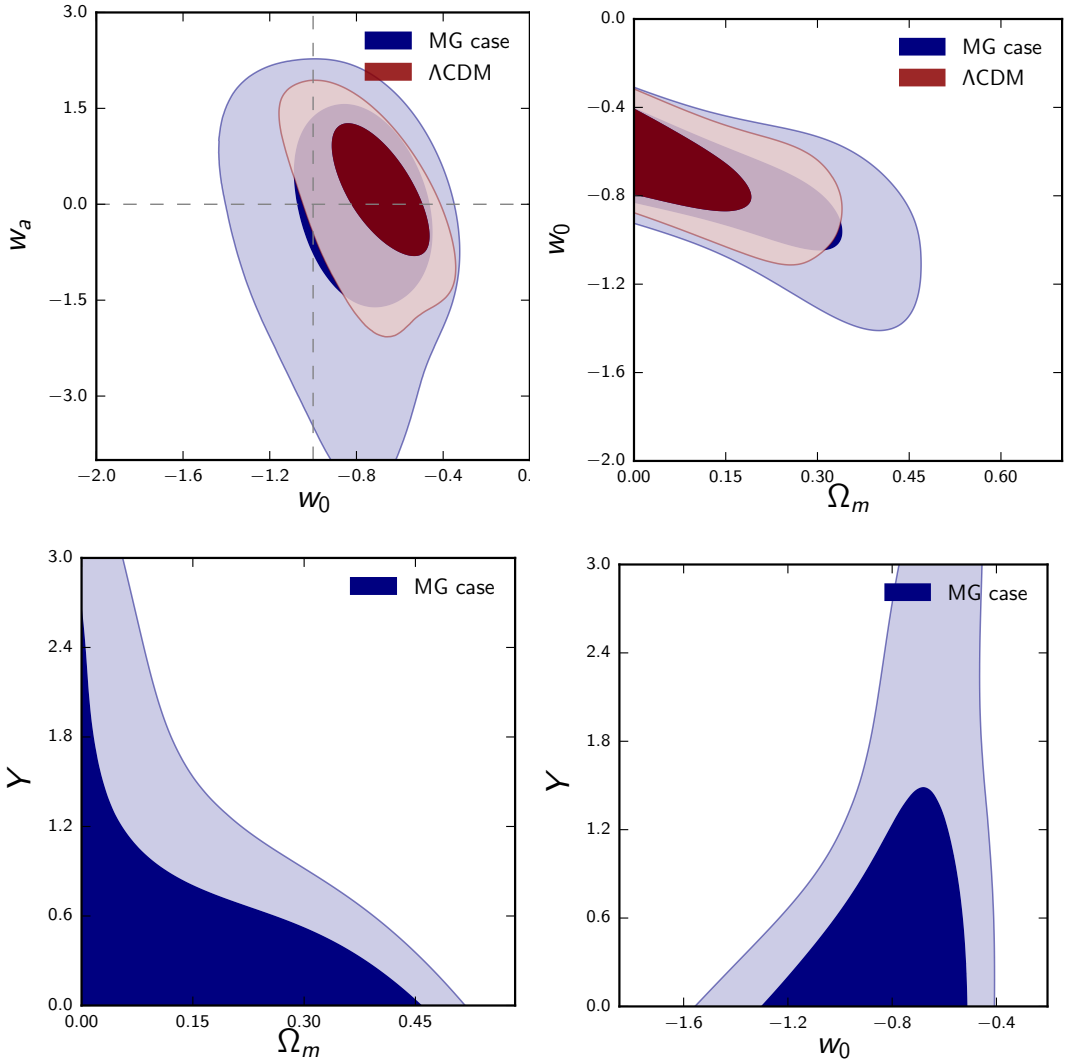


Figure 1. Top panels: 1σ and 2σ confidence-level contours for the parameters $\{w_0, w_a\}$ (top left), $\{\Omega_{m,0}, w_0\}$ (top right). Bottom panels: confidence-level contours for the parameters $\{\Omega_{m,0}, Y\}$ (bottom left) and $\{w_0, Y\}$ (bottom right). Red contours refer to the Λ CDM analysis, while blue ones refer to the full case.

and weak lensing has been estimated.

The fiducial values and errors for $f\sigma_8$ and E are summarized in Table 3 (see also Fig. 4). As with currently available data, we analyze the Λ CDM and the MG cases, investigating how the additional parameters affect the achievable constraints. We use now the χ^2 described in Eq. (3.4), sampling the parameter space with the techniques mentioned at the end of Section 2.

As done for the currently available data, we assume that the additional parameters Y and α , together with the galaxy bias b , are not scale dependent; for this reason we consider only the redshift binning, without including any binning in k . An explicit scale dependence for Y parameter is instead considered in Section 6 of this paper, where therefore the predicted

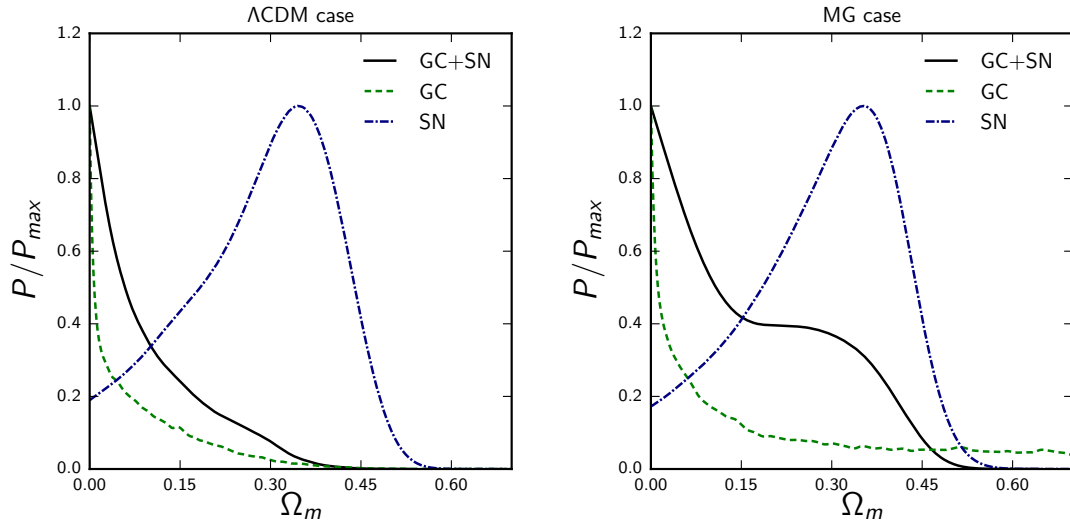


Figure 2. Posterior distribution of Ω_m in the Λ CDM (left panel) and MG (right panel) cases, using growth data (green dashed line), supernovae data (blue dot-dashed line) and their combination (black solid line).

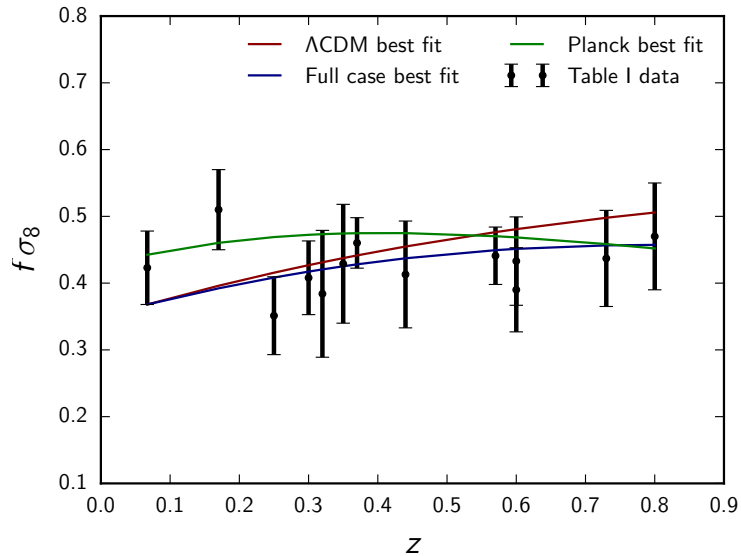


Figure 3. Currently available $f\sigma_8(z)$ data compared with the theoretical prediction using Planck 2015 best fit parameters (green line) and with the Λ CDM and MG cases best fits (respectively red and blue lines).

observations performed by the Euclid survey are binned also in scale.

SKA mission

As a comparison with Euclid, we also consider another almost contemporary facility, the Square Kilometre Array (SKA), which is a giant radio telescope array which will be built across two sites, in South Africa and in Western Australia. Its main aim will be to probe

Fiducial			Euclid	
\bar{z}	E	f	ΔE (68% c.l.)	$\Delta f\sigma_8$ (68% c.l.)
0.6	1.37	0.469	0.011	0.0078
0.8	1.53	0.457	0.021	0.0057
1.0	1.72	0.438	0.024	0.0045
1.2	1.92	0.417	0.024	0.0038
1.4	2.14	0.396	0.025	0.0035
1.8	2.62	0.354	0.034	0.0025

Table 3. Fiducial values and errors for $f\sigma_8$ and E for the Euclid survey, combining weak lensing and galaxy clustering measurements (from [6]).

the nature of dark energy by mapping out large-scale structures, primarily using the 21-cm emission line of neutral hydrogen (HI) to measure the galaxy’s redshift with high precision [32].

The SKA project will consist of two phases, denoted SKA1 and SKA2 in the following. Phase 1 will be formed by three different arrays: SKA1-MID, SKA1-SUR, which are dish arrays with a mid-frequency ($\nu \lesssim 1.4$ GHz) receivers and low/intermediate redshifts and SKA1-LOW which is an aperture array with a lower frequency ($\nu < 350$ MHz) and higher redshifts. The LOW will be capable to detect HI emission only for $z \geq 3$ by using intensity mapping (IM) rather than a galaxy survey, so we will not consider it here. The SKA1 survey (for either MID and SUR) will cover 5,000 deg² area and it will detect about 5×10^6 HI galaxies up to $z \sim 0.5$. The second phase, SKA2, planned for the late 2020s, will have a sensitivity around 10 times the one of SKA1 and should be capable of detecting about 10^9 HI galaxies over a 30,000 deg² area, up to $z \sim 2.0$.

For both cases, we follow the procedure described in [33] and obtain the galaxy redshift distribution functions (dN/dz) and the bias redshift evolution ($b(z)$) as

$$\frac{dN}{dz}(z) = 10^{c_1} z^{c_2} \exp(-c_3 z) \quad (5.1)$$

$$b(z) = c_4 \exp(c_5 z) \quad (5.2)$$

where the values of the c_i parameters are obtained from [33].

In [33], constraints on dark energy equation of state parameters w_0 and w_a and on the spatial curvature parameter Ω_K are obtained using forecast BAO measurements for SKA1 and SKA2 and these are compared with a Euclid like H α galaxy survey. The interesting point is that SKA2 outperforms Euclid by a factor around 2 due to the fact that it has a double area and an additional redshift bin below Euclid’s minimum redshift. As for Euclid, we build forecast datasets for both SKA1 and SKA2 observations of galaxy clustering, dividing the redshift range $0 \leq z \leq 2.5$ in six equispaced bins, which are reported in Table 4 (see also Fig. 4), and we analyze these in the Λ CDM and MG cases. As done for Euclid observations, we do not consider a k -binning for this case.

SKA will also be able to perform shear measurements as the Euclid survey [34–36]. Therefore, following the same procedure used for Euclid and the SKA shear specifications [34], we include forecast shear measurements for both SKA1 and SKA2.

Fiducial			SKA1		SKA2	
\bar{z}	E	$f\sigma_8$	ΔE (68% c.l.)	$\Delta f\sigma_8$ (68% c.l.)	ΔE (68% c.l.)	$\Delta f\sigma_8$ (68% c.l.)
0.21	1.10	0.455	0.03	0.022	0.002	0.008
0.63	1.39	0.468	0.02	0.019	0.001	0.003
1.05	1.77	0.433	0.12	0.5	0.007	0.002
1.47	2.22	0.388	0.16	39	0.02	0.003
1.89	2.73	0.346	0.69	$3.4 \cdot 10^3$	0.02	0.006
2.31	3.29	0.309	1.00	$3.0 \cdot 10^5$	0.09	0.04

Table 4. Fiducial values and SKA1 and SKA2 errors for $f\sigma_8$ and E combining weak lensing and galaxy clustering measurements.

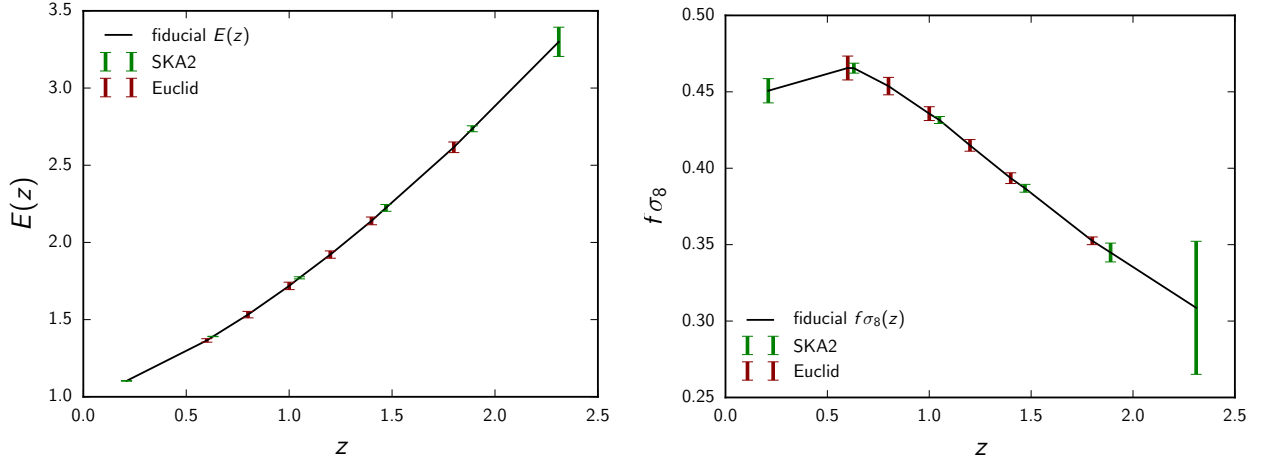


Figure 4. Fiducial cosmology predictions for $E(z)$ and $f\sigma_8(z)$ (black lines) and forecast errors obtained with specifications for SKA2 (green error bars) and Euclid Full (red error bars).

Future Supernovae survey

On top of the information brought by Weak Lensing and Galaxy Clustering, we assume that constraints on the background are also imposed by a future supernovae Ia survey; we consider observations in the redshift range $0 < z < 2.5$ and we divide the interval in the same bins used for the SKA survey (but with the initial redshift $z = 0$ instead of 0.05). We also assume that, in this range, the total number of observed SN is $n_{SN} = 10^5$ as expected for LSST survey [37], taking as a reference the Union 2.1 [38] catalogue for the distribution of data in each bin and for the average magnitude errors. Notice that with this choice the last two SKA bins do not include any supernova.

Given these survey specifications we obtain the Fisher matrix for supernovae observation and the χ^2 obtained from these at each step of the MCMC is then added to the one obtained by the combination WL+GC in order to construct a joint posterior for the free parameters.

Results

Table 5 and Table 6 report, respectively, the results obtained in the Λ CDM limit ($Y = 1$ and $\alpha = 1$) and those for the full MG analysis, where both Y and α are free parameters. These

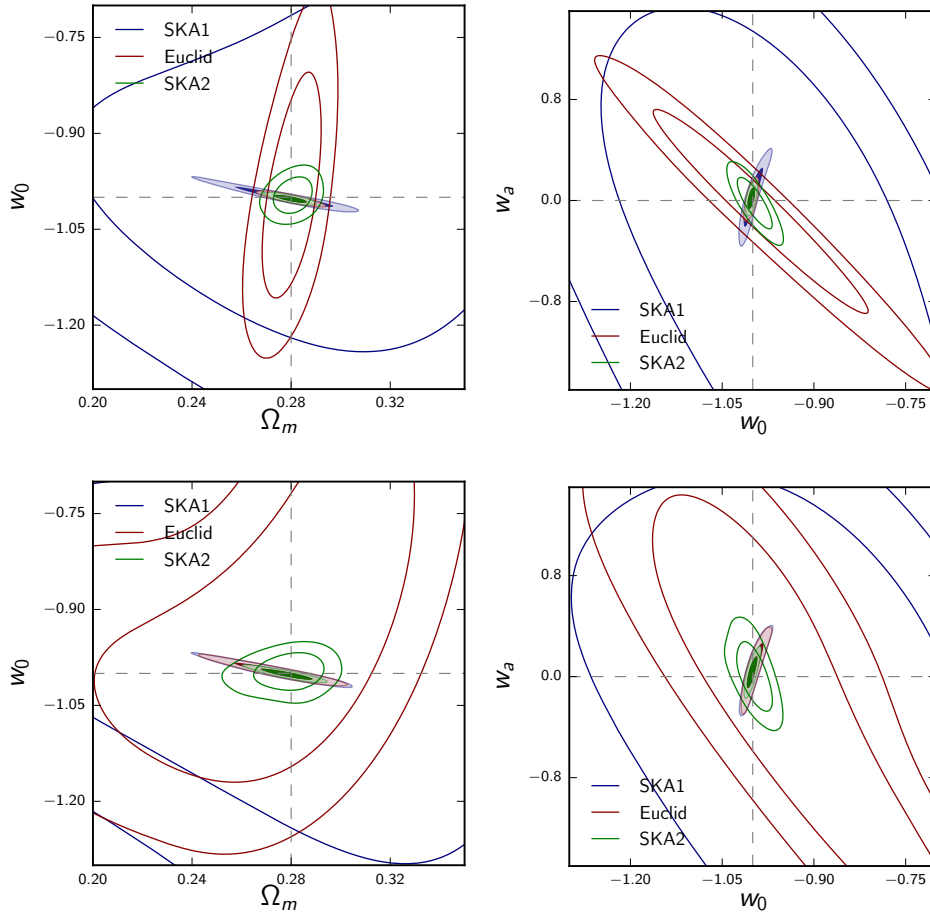


Figure 5. 1σ and 2σ confidence-level contours for the standard cosmological parameters pairs $\{\Omega_{m,0}, w_0\}$ (left column) and $\{w_0, w_a\}$ (right column). Top panels refer to the Λ CDM analysis, while the bottom ones describe results obtained in the MG case. We show all the considered surveys: SKA1 (blue) Euclid (red) and SKA2 (green). Empty contours refer to the GC+WL combination, while full contours also include SN information. Grey dashed lines show the fiducial values of the parameters.

Forecast data: Λ CDM case	SKA1	Euclid	SKA2
$\Omega_{m,0}$	$0.277^{+0.015}_{-0.010}$	0.2800 ± 0.0056	$0.2799^{+0.0044}_{-0.0040}$
w_0	$-0.9998^{+0.0074}_{-0.012}$	-1.0022 ± 0.0050	-1.0026 ± 0.0040
w_a	0.03 ± 0.16	0.011 ± 0.071	0.017 ± 0.053

Table 5. Marginalized values and $1-\sigma$ errors on the free parameters for forecast data (which includes Euclid, SKA1 and SKA2) in the Λ CDM case.

results are also shown graphically in Fig. 5 where the top panels contain the 2D contour plots obtained in Λ CDM, while the bottom ones refer to the MG case.

It is immediate to see how, although all the considered data combinations are expected to be extremely precise in measuring the expansion history of the Universe, constraints brought

Forecast data: full case	SKA1	Euclid	SKA2
$\Omega_{m,0}$	$0.275^{+0.014}_{-0.011}$	$0.276^{+0.012}_{-0.0095}$	$0.2782^{+0.0072}_{-0.0062}$
α	> -0.0431	$1.17^{+0.61}_{-1.0}$	$1.12^{+0.30}_{-0.45}$
w_0	$-0.9986^{+0.0084}_{-0.012}$	$-0.9987^{+0.0069}_{-0.0098}$	$-1.0013^{+0.0051}_{-0.0061}$
w_a	0.06 ± 0.15	0.05 ± 0.13	0.036 ± 0.084
Y	$1.09^{+0.45}_{-0.32}$	$0.98^{+0.35}_{-0.14}$	$1.02^{+0.13}_{-0.11}$

Table 6. Marginalized values and $1-\sigma$ errors on the free parameters for forecast data (which includes Euclid, SKA1 and SKA2) when MG parameters are allowed to vary.

by galaxy clustering and weak lensing on the standard cosmological parameters are degraded when MG parameters are included in the analysis; this can be noticed comparing the empty contours of the top and bottom panels of Fig. 5. In the Euclid case for example, the errors on $\Omega_{m,0}$, w_0 and w_a increase respectively by roughly 5, 2 and 3 times. This is due, as already discussed for currently available data in the previous section, to the degeneracies between standard parameters and Y and α , which are shown by the empty contours of Fig. 6. The net effect of allowing modified gravity is therefore to make more expansion histories viable despite the extreme sensitivity of future surveys.

However, as SN information is not affected by the MG parameters, which modify only the linear perturbations, its inclusion strongly helps to break degeneracies, as it can be seen in the filled contours of Fig. 6 and in Table 6.

It is interesting to notice how the current constraints on MG parameters significantly improve using forecasts for these experiments; this means that despite the degeneracies highlighted here, future surveys will be able to significantly reduce the parameter space regions allowed for modified gravity theories.

Figure 7 shows the posterior distribution on Y obtained using the Euclid full dataset (i.e. with the inclusion of supernovae) both with a varying α and α fixed to 1. In this second case we also show the posterior obtained without marginalizing a priori on σ_8 ; in this case we use the χ^2 of Eq. (3.2), with a free-to-vary σ_8 derived from the cosmological parameters assuming GR. In this plot we notice, as expected, how the constraint on Y are much tighter when $\alpha = 1$ with respect to the general initial conditions case. We notice also how the inclusion of σ_8 in the analysis slightly improves further the constraint on Y although relying on a specific assumption of the gravity theory.

6 A cosmological exclusion plot

In this section we wish to obtain an exclusion plot, i.e. the region of the parameter space that a future redshift surveys can achieve, in analogy to what already done in [11]. We remind that, in the quasi-static limit of the Horndeski theory, the expression for Y is given by Eq. (2.6). If we perform a Fourier anti-transformation of this equation, we obtain a Yukawa-like gravitational potential

$$\Psi(r) = -\frac{G_0 M}{r} h_1 \left(1 + Q e^{-r/\lambda}\right) \quad (6.1)$$

where $h_5 = (1 + Q)\lambda^2$ and $h_3 = \lambda^2$ (notice that $M h_1$ is the observable, not h_1 alone), and where the mass M is to be interpreted as the gravitational mass of a source at the origin. Here G_0 is the gravitational constant one would measure in laboratory where the effects of

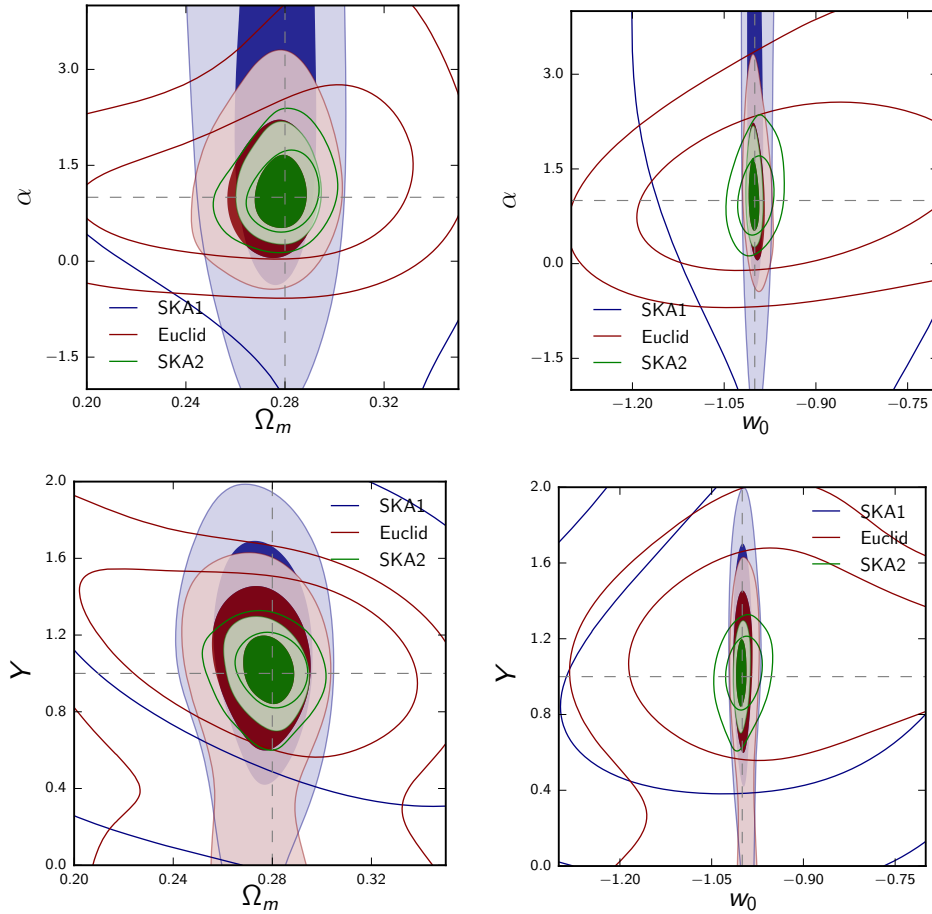


Figure 6. 1σ and 2σ confidence-level contours for the parameters $\{\Omega_{m,0}, \alpha\}$ (top left), $\{w_0, \alpha\}$ (top right), $\{\Omega_{m,0}, Y\}$ (bottom left) and $\{w_0, Y\}$ (bottom right). We show all the considered surveys: SKA1 (blue) Euclid (red) and SKA2 (green). Empty contours refer to the GC+WL combination, while full contours also include SN information. Grey dashed lines show the fiducial values of the parameters.

the modification of gravity are assumed to be screened or baryons to be uncoupled. Now, we want to solve Eq. (2.5) in the quasi-static Horndeski result coupled to the background defined in Eq. (2.3), so in total, we have seven parameters: the strength Q and the range λ of the Yukawa term (we assume that they are constant in the observed range), h_1 , the initial conditions α and $\Omega_{m,0}, w_0, w_a$. If one were to satisfy the present-time constraints on $(\dot{G}M)/GM$ at all times, then $h_1 = 1$ with great precision. As we already remarked, however, this extrapolation of present constraints to the past is unwarranted and we leave therefore h_1 as a free parameter to be marginalized over.

We reproduce the exclusion plot only for the Euclid and SKA2 cases since, as we have seen before, they are those that best constrain the parameters. In order to solve Eq. (2.5), we need to have a minimum of three k -bins for every value of the redshift. We take the minimum binning value of k as $k_{min} = 0.007 h/\text{Mpc}$ (the results are very much insensitive to this choice) and the value of the highest k is conservatively chosen to be below the scale of non-linearity

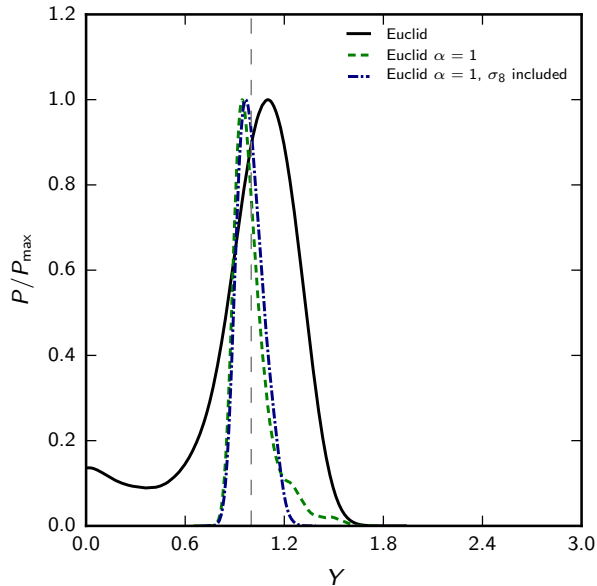


Figure 7. Posterior distribution for the Y parameter recovered marginalizing over σ_8 and varying both Y and α (black solid line) or fixing $\alpha = 1$ (green dashed line). The posterior is also shown with a free to vary σ_8 without marginalizing it out of the likelihood (blue dot-dashed line).

at the redshift of the first bin for the Euclid case. For simplicity, we assume that the k -values are the same for all the redshift bins ($k_{min} - k_1 : 0.007 - 0.022$, $k_1 - k_2 : 0.022 - 0.063$, $k_2 - k_{max} = 0.063 - 0.180$) for both surveys. In Table 7 we display the fiducial values and errors for $f\sigma_8$ and E at every redshift and every k -bin for the Euclid case and in Table 8 for the SKA2-full. We numerically solve Eq. (2.5) inserting the value of k corresponding to the central value of each k -bin and we vary the value of λ from 0 to 120 Mpc/h ; for every step, we calculate the errors on Q at 68% and 95% of c.l., marginalizing over all the other parameters. The region which is outside the errors on Q is therefore the region that a future survey will be able to rule out. The parameters Q and λ are the cosmological analog of the parameters employed in laboratory experiments to test deviations from Newtonian gravity, see e.g. [39].

Fig. 8 shows the region that the Euclid survey (left panel) and SKA2 survey (right panel) can exclude. It appears that they are very similar. For very small values of λ , the strength Q is unconstrained, since in this limit the fifth-force effects decay at small distances. Q is weakly constrained also at very large λ since in this limit Y becomes scale independent and the overall constant h_1 is marginalised over. The constraints are therefore maximized at intermediate values $10\text{Mpc}/h < \lambda < 50\text{Mpc}/h$. In this regime, both surveys will constrain Q to be smaller than 0.2-0.3 (68% c.l.)

In the popular class of $f(R)$ models, one has $Q = 1/3$ and the range $\lambda = 1/m$ where m is the mass of the scalaron given by

$$m^2 = \frac{R}{3} \left(\frac{1 + f_{,R}}{R f_{,RR}} - 1 \right) \quad (6.2)$$

where $f_{,R}, f_{,RR}$ are derivatives with respect to R . Moreover, $h_1 = 1/(1 + f_{,R})$. Often constraints on $f(R)$ are obtained for specific models and fixing the background to be ΛCDM ,

\bar{z}	i	$f\sigma_8(z)$	$\Delta f\sigma_8(z)$	E	ΔE
	1		0.069		
0.6	2	0.469	0.017	1.37	0.003
	3		0.009		
	1		0.005		
0.8	2	0.457	0.013	1.53	0.03
	3		0.007		
	1		0.044		
1.0	2	0.438	0.011	1.72	0.06
	3		0.005		
	1		0.039		
1.2	2	0.417	0.009	1.92	0.010
	3		0.004		
	1		0.035		
1.4	2	0.396	0.008	2.14	0.018
	3		0.004		
	1		0.019		
1.8	2	0.354	0.005	2.62	0.035
	3		0.003		

Table 7. Fiducial values and relative errors for $f\sigma_8$ data at every redshift \bar{z} and every k -bin (labeled with the index i , from [6]), for the Euclid survey.

[40, 41]. Our exclusion plot allows us to remove these assumptions since we do not fix the modified gravity model and we marginalize over the background. From Fig. 8 we see that $f(R)$ models can be ruled out only if the range $\lambda = 1/m$ is within 10 – 40 Mpc/ h at 95% c.l. and 5 – 70 Mpc/ h at 68% c.l. .

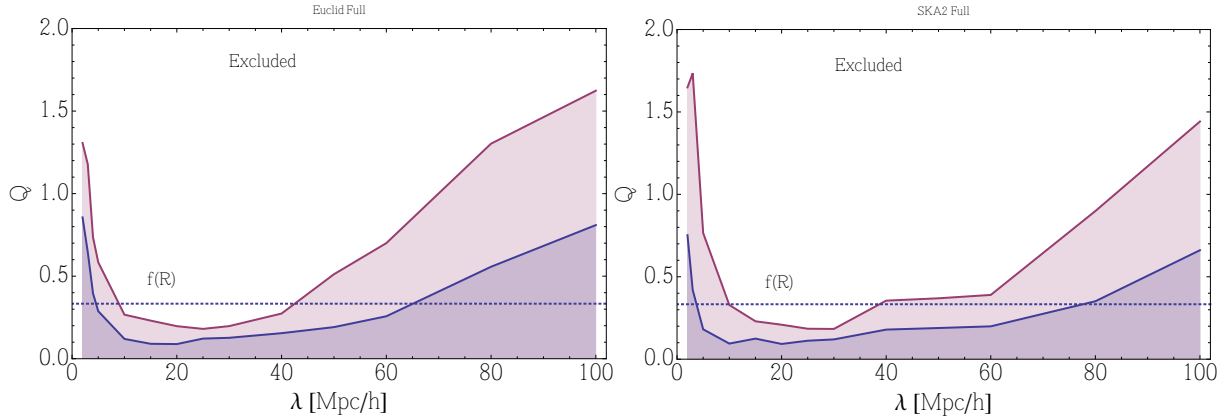


Figure 8. Forecast of a cosmological exclusion plot for the Euclid (left panel) and for the SKA2 (right panel) surveys. In both cases, the darker region is the 68% c.l. region, the lighter one is the 95% c.l. region. The dotted line is the value of Q in $f(R)$ models.

\bar{z}	i	$f\sigma_8(z)$	$\Delta f\sigma_8(z)$	E	ΔE
	1		0.060		
0.26	2	0.459	0.015	1.13	0.0003
	3		0.010		
	1		0.030		
0.75	2	0.460	0.007	1.48	0.0009
	3		0.004		
	1		0.025		
1.25	2	0.412	0.006	1.97	0.0043
	3		0.003		
	1		0.026		
1.75	2	0.359	0.006	2.55	0.016
	3		0.003		
	1		0.038		
2.25	2	0.314	0.011	3.21	0.020
	3		0.008		
	1		0.12		
2.75	2	0.277	0.049	3.93	0.095
	3		0.044		

Table 8. Fiducial values and relative errors for $f\sigma_8$ data at every redshift \bar{z} and every k -bin (labeled with the index i), for the SKA2 survey.

7 Conclusions

In this paper we investigated deviations from the standard Poisson’s equation in terms of general modifications of the gravitational theory, parametrized through an effective gravitational constant Y . With respect to previous results we make a further attempt towards a model independent approach, using general initial conditions, encoded in the α parameter, and marginalizing σ_8 out of the likelihood, thus removing the need of a choice of the shape of the power spectrum. We assumed the parameters Y and α to be constant or, in the case of Y , to follow a Horndeski behavior. Alongside the modified growth of perturbations, we also assume a general expansion history described by $w(a) = w_0 + w_a(1 - a)$.

As explained in the Introduction and in the forecast section, one should be careful in comparing our results to similar analyses: generally speaking, the more one tries to be model-independent, the more is likely to obtain weaker constraints. These constraints are however by construction more robust in the sense that they stay the same even when other models of, e.g., initial conditions or bias, are assumed.

In the constant parameters assumption, we analyzed this general parametrization with currently available supernovae and galaxy surveys, investigating the effect of deviations from the standard growth and expansion history. In order to preserve the generality of our approach, we marginalize an overall amplitude out of the data when computing our likelihood, as this depends on unknown initial conditions. We find that current data are not able to constrain the modified gravity parameters with good precision, as α is constrained with a $\approx 300\%$ error, while only an upper bound can be obtained on Y . Interestingly, we find that the growth-rate data prefer $\Omega_{m,0}$ to assume small values, while supernovae data support

a maximum likelihood $\Omega_{m,0} \approx 0.3$. The combined analysis still prefers low values of the matter density, but the effect of supernovae is to make more likely values excluded by the growth-data-only analysis, in the modified gravity case.

We also forecast the performances of two future experiments: SKA, in the SKA1 and SKA2 configurations, and Euclid. In both cases we combine the expected information coming from galaxy clustering and weak lensing, and we include also a forecast for a future SN survey. It is possible to notice how these future experiments will significantly improve our knowledge of gravity, as possible deviations from the standard GR will be constrained with a $\approx 30\%$ error on Y and a $\approx 70\%$ one on α in the most sensitive case considered here (SKA2).

Finally we adopt a Horndeski form for Y , i.e. a Yukawa-like correction to the Newtonian gravitational potential. The constraints imposed by future experiments are represented as a cosmological exclusion plot between the parameters Q and λ , i.e. the strength and range of the Yukawa force introduced by the modification of gravity. We find that the strength will be constrained to be less than 0.2 at 68% c.l. of the Newtonian gravitational strength for both the Euclid and the SKA2 cases if the interaction range is around 10-50 Mpc/ h . This constraint will be sufficient to rule out all $f(R)$ models with a range in this regime.

8 Acknowledgments

L. Taddai thanks "Fondazione Angelo della Riccia" for financial support. We thank DFG for support through the Transregio 33 project "The Dark Universe".

References

- [1] Adam G. Riess et al. Observational evidence from supernovae for an accelerating universe and a cosmological constant. *Astron. J.*, 116:1009–1038, 1998.
- [2] S. Perlmutter et al. Measurements of Omega and Lambda from 42 high redshift supernovae. *Astrophys. J.*, 517:565–586, 1999.
- [3] Luca Amendola and Shinji Tsujikawa. *Dark Energy: Theory and Observations*. Cambridge University Press, 2010.
- [4] L. Amendola, S. Appleby, D. Bacon, T. Baker, M. Baldi, N. Bartolo, A. Blanchard, C. Bonvin, S. Borgani, E. Branchini, C. Burrage, S. Camera, C. Carbone, L. Casarini, M. Cropper, C. deRham, C. di Porto, A. Ealet, P. G. Ferreira, F. Finelli, J. Garcia-Bellido, T. Giannantonio, L. Guzzo, A. Heavens, L. Heisenberg, C. Heymans, H. Hoekstra, L. Hollenstein, R. Holmes, O. Horst, K. Jahnke, T. D. Kitching, T. Koivisto, M. Kunz, G. La Vacca, M. March, E. Majerotto, K. Markovic, D. Marsh, F. Marulli, R. Massey, Y. Mellier, D. F. Mota, N. Nunes, W. Percival, V. Pettorino, C. Porciani, C. Quercellini, J. Read, M. Rinaldi, D. Sapone, R. Scaramella, C. Skordis, F. Simpson, A. Taylor, S. Thomas, R. Trotta, L. Verde, F. Vernizzi, A. Vollmer, Y. Wang, J. Weller, and T. Zlosnik. Cosmology and fundamental physics with the Euclid satellite. *ArXiv e-prints*, June 2012.
- [5] L. Amendola, M. Kunz, M. Motta, I. D. Saltas, and I. Sawicki. Observables and unobservables in dark energy cosmologies. *Phys. Rev. D*, 87(2):023501, January 2013.
- [6] Luca Amendola, Simone Fogli, Alejandro Guarnizo, Martin Kunz, and Adrian Vollmer. Model-independent constraints on the cosmological anisotropic stress. *Phys.Rev.*, D89:063538, 2014.
- [7] Antonio De Felice, Tsutomu Kobayashi, and Shinji Tsujikawa. Effective gravitational couplings for cosmological perturbations in the most general scalar-tensor theories with second-order field equations. *Phys.Lett.*, B706:123–133, 2011.

- [8] Luca Amendola, Martin Kunz, Mariele Motta, Ippocratis D. Saltas, and Ignacy Sawicki. Observables and unobservables in dark energy cosmologies. *Phys.Rev.*, D87:023501, 2013.
- [9] Alessandra Silvestri, Levon Pogosian, and Roman V. Buniy. A practical approach to cosmological perturbations in modified gravity. 2013.
- [10] Ignacy Sawicki and Emilio Bellini. Limits of quasistatic approximation in modified-gravity cosmologies. *Phys. Rev.*, D92(8):084061, 2015.
- [11] Laura Taddei and Luca Amendola. A cosmological exclusion plot: Towards model-independent constraints on modified gravity from current and future growth rate data. *JCAP*, 1502(02):001, 2015.
- [12] Michel Chevallier and David Polarski. Accelerating universes with scaling dark matter. *Int.J.Mod.Phys.*, D10:213–224, 2001.
- [13] Antony Lewis and Sarah Bridle. Cosmological parameters from CMB and other data: A Monte Carlo approach. *Phys. Rev.*, D66:103511, 2002.
- [14] M. Betoule et al. Improved cosmological constraints from a joint analysis of the SDSS-II and SNLS supernova samples. *Astron.Astrophys.*, 568:A22, 2014.
- [15] Edward Macaulay, Ingunn Kathrine Wehus, and Hans Kristian Eriksen. A Lower Growth Rate from Recent Redshift Space Distortions than Expected from Planck. 2013.
- [16] Surhud More, Hironao Miyatake, Rachel Mandelbaum, Masahiro Takada, David Spergel, et al. The Weak Lensing Signal and the Clustering of BOSS Galaxies: Cosmological Constraints. 2014.
- [17] Florian Beutler, Chris Blake, Matthew Colless, D. Heath Jones, Lister Staveley-Smith, et al. The 6dF Galaxy Survey: $z = 0$ measurement of the growth rate and σ_8 . *Mon.Not.Roy.Astron.Soc.*, 423:3430–3444, 2012.
- [18] Lado Samushia, Will J. Percival, and Alvise Raccanelli. Interpreting large-scale redshift-space distortion measurements. *Mon.Not.Roy.Astron.Soc.*, 420:2102–2119, 2012.
- [19] Rita Tojeiro, W.J. Percival, J. Brinkmann, J.R. Brownstein, D. Eisenstein, et al. The clustering of galaxies in the SDSS-III Baryon Oscillation Spectroscopic Survey: measuring structure growth using passive galaxies. *Mon.Not.Roy.Astron.Soc.*, 424:2339–2344, 2012.
- [20] Chris Blake, Sarah Brough, Matthew Colless, Carlos Contreras, Warrick Couch, et al. The WiggleZ Dark Energy Survey: Joint measurements of the expansion and growth history at $z < 1$. *Mon.Not.Roy.Astron.Soc.*, 425:405–414, 2012.
- [21] S. de la Torre, L. Guzzo, J.A. Peacock, E. Branchini, A. Iovino, et al. The VIMOS Public Extragalactic Redshift Survey (VIPERS). Galaxy clustering and redshift-space distortions at $z=0.8$ in the first data release. 2013.
- [22] Will J. Percival et al. The 2dF Galaxy Redshift Survey: Spherical harmonics analysis of fluctuations in the final catalogue. *Mon.Not.Roy.Astron.Soc.*, 353:1201, 2004.
- [23] Yong-Seon Song and Will J. Percival. Reconstructing the history of structure formation using Redshift Distortions. *JCAP*, 0910:004, 2009.
- [24] Chia-Hsun Chuang and Yun Wang. Modeling the Anisotropic Two-Point Galaxy Correlation Function on Small Scales and Improved Measurements of $H(z)$, $D_A(z)$, and $\beta(z)$ from the Sloan Digital Sky Survey DR7 Luminous Red Galaxies. *Mon.Not.Roy.Astron.Soc.*, 435:255–262, 2013.
- [25] Chia-Hsun Chuang, Francisco Prada, Florian Beutler, Daniel J. Eisenstein, Stephanie Escoffier, et al. The clustering of galaxies in the SDSS-III Baryon Oscillation Spectroscopic Survey: single-probe measurements from CMASS and LOWZ anisotropic galaxy clustering. 2013.

- [26] Florian Beutler et al. The clustering of galaxies in the SDSS-III Baryon Oscillation Spectroscopic Survey: Testing gravity with redshift-space distortions using the power spectrum multipoles. 2013.
- [27] Lado Samushia, Beth A. Reid, Martin White, Will J. Percival, Antonio J. Cuesta, et al. The Clustering of Galaxies in the SDSS-III Baryon Oscillation Spectroscopic Survey (BOSS): measuring growth rate and geometry with anisotropic clustering. 2013.
- [28] Beth A. Reid, Hee-Jong Seo, Alexie Leauthaud, Jeremy L. Tinker, and Martin White. A 2.5space clustering of SDSS-III CMASS galaxies. 2014.
- [29] P. A. R. Ade et al. Planck 2015 results. XIII. Cosmological parameters. 2015.
- [30] R. Laureijs, J. Amiaux, S. Arduini, J. . Auguères, J. Brinchmann, R. Cole, M. Cropper, C. Dabin, L. Duvet, A. Ealet, and et al. Euclid Definition Study Report. *ArXiv e-prints*, October 2011.
- [31] L. Pozzetti, C. M. Hirata, J. E. Geach, A. Cimatti, C. Baugh, O. Cucciati, A. Merson, P. Norberg, and D. Shi. Modelling the number density of H α emitters for future spectroscopic near-IR space missions. *Astron. Astrophys.*, 590:A3, 2016.
- [32] Filipe Batoni Abdalla et al. Cosmology from HI galaxy surveys with the SKA. *PoS, AASKA14:017*, 2015.
- [33] S. Yahya, P. Bull, M. G. Santos, M. Silva, R. Maartens, P. Okouma, and B. Bassett. Cosmological performance of SKA HI galaxy surveys. *Mon. Not. Roy. Astron. Soc.*, 450:2251–2260, 2015.
- [34] Ian Harrison, Stefano Camera, Joe Zuntz, and Michael L. Brown. SKA Weak Lensing I: Cosmological Forecasts and the Power of Radio-Optical Cross-Correlations. 2016.
- [35] Anna Bonaldi, Ian Harrison, Stefano Camera, and Michael L. Brown. SKA Weak Lensing II: Simulated Performance and SurveyDesign Considerations. 2016.
- [36] Stefano Camera, Ian Harrison, Anna Bonaldi, and Michael L. Brown. SKA Weak Lensing III: Added Value of Multi-Wavelength Synergies for the Mitigation of Systematics. 2016.
- [37] J. Anthony Tyson. Large synoptic survey telescope: Overview. *Proc. SPIE Int. Soc. Opt. Eng.*, 4836:10–20, 2002.
- [38] R. Amanullah et al. Spectra and Light Curves of Six Type Ia Supernovae at $0.511 < z < 1.12$ and the Union2 Compilation. *Astrophys. J.*, 716:712–738, 2010.
- [39] D. J. Kapner, T. S. Cook, E. G. Adelberger, J. H. Gundlach, B. R. Heckel, C. D. Hoyle, and H. E. Swanson. Tests of the Gravitational Inverse-Square Law below the Dark-Energy Length Scale. *Physical Review Letters*, 98(2):021101, January 2007.
- [40] Jason Dossett, Bin Hu, and David Parkinson. Constraining models of f(R) gravity with Planck and WiggleZ power spectrum data. *JCAP*, 1403:046, 2014.
- [41] Alireza Hojjati, Aaron Plahn, Alex Zucca, Levon Pogossian, Philippe Brax, Anne-Christine Davis, and Gong-Bo Zhao. Searching for scalar gravitational interactions in current and future cosmological data. *Phys. Rev.*, D93(4):043531, 2016.